Generalization of Wigner Time Delay to Sub-Unitary Scattering Systems

Lei Chen, 1,2,* Steven M. Anlage, 1,2,† and Yan V. Fyodorov^{3,4,‡}

¹ Quantum Materials Center, Department of Physics,
University of Maryland, College Park, MD 20742, USA

² Department of Electrical and Computer Engineering,
University of Maryland, College Park, MD 20742, USA

³ Department of Mathematics, King's College London, London WC26 2LS, United Kingdom

⁴ L. D. Landau Institute for Theoretical Physics, Semenova 1a, 142432 Chernogolovka, Russia
(Dated: April 27, 2021)

We introduce a complex generalization of Wigner time delay τ for sub-unitary scattering systems. Theoretical expressions for complex time delay as a function of excitation energy, uniform and non-uniform loss, and coupling, are given. We find very good agreement between theory and experimental data taken on microwave graphs containing an electronically variable lumped-loss element. We find that time delay and the determinant of the scattering matrix share a common feature in that the resonant behavior in $\text{Re}[\tau]$ and $\text{Im}[\tau]$ serves as a reliable indicator of the condition for Coherent Perfect Absorption (CPA). This work opens a new window on time delay in lossy systems and provides a means to identify the poles and zeros of the scattering matrix from experimental data. The results also enable a new approach to achieving CPA at an arbitrary energy/frequency in complex scattering systems.

Introduction. In this paper we consider the general problem of scattering from a complex system by means of excitations coupled through one or more scattering channels. The scattering matrix S describes the transformation of a set of input excitations $|\psi_{\rm in}\rangle$ on M channels into the set of outputs $|\psi_{\rm out}\rangle$ as $|\psi_{\rm out}\rangle = S |\psi_{\rm in}\rangle$.

A measure of how long the excitation resides in the interaction region is provided by the time delay, related to the energy derivative of the scattering phase(s) of the system. This quantity and its variation with energy and other parameters can provide useful insights into the properties of the scattering region and has attracted research attention since the seminal works by Wigner [1] and Smith [2]. A review on theoretical aspects of time delays with emphasis to solid state applications can be found in [3]. Various aspects of time delay have recently been shown to be of direct experimental relevance for manipulating wave fronts in complex media [4–6]. Time delays are also long known to be directly related to the density of states of the open scattering system, see discussions in [3] and more recently in [7, 8].

For the case of flux-conserving scattering in systems with no losses, the S-matrix is unitary and its eigenvalues are phases $e^{i\theta_a}, a=1,2,...,M$. These phases are functions of the excitation energy E and one can then define several different measures of time delay, see e.g. [3,9], such as partial time delays associated with each channel $\tau_a=d\theta_a/dE$, the proper time delays which are the eigenvalues of the Wigner-Smith matrix $\hat{Q}=i\hbar\frac{dS^\dagger}{dE}S$, and the Wigner delay time which is the average of all the partial time delays $(\tau_{\rm W}=\frac{1}{M}\sum_{a=1}^{M}\tau_a=\frac{1}{M}Tr[\hat{Q}])$.

A rich class of systems in which properties of various time delays enjoyed thorough theoretical attention is scattering of short-wavelength waves from classically chaotic systems, e.g. billiards with ray-chaotic dynamics or particles on graphs, e.g. such as considered in [10]. Various examples of chaotic wave scattering (quantum or classical) have been observed in nuclei, atoms, molecules, ballistic two-dimensional electron gas billiards, and most extensively in microwave experiments [11–16]. In such systems time delays have been measured starting from the pioneering work [17], followed over the last three decades by measurement of the statistical properties of time delay through random media [18, 19] and microwave billiards [20]. Wigner time delay for an isolated resonance described by an S-matrix pole at complex energy $E_0 - i\Gamma$ has a value of $Q = 2\hbar/\Gamma$ on resonance, hence studies of the imaginary part of the S-matrix poles probe one aspect of time delay [21–26]. In the meantime, the Wigner-Smith operator (WSO) was utilized to identify minimally-dispersive principal modes in coupled multimode systems [27, 28]. A similar idea was used to create particle-like scattering states as eigenstates of the WSO [4, 29, 30]. A generalization of the WSO allowed maximal focus on, or maximal avoidance of, a specific target inside a multiple scattering medium [6, 31].

Time delays in wave-chaotic scattering are expected to be extremely sensitive to variations of excitation energy and scattering system parameters, and will display universal fluctuations when considering an ensemble of scattering systems with the same general symmetry. Universality of fluctuations allows them to be efficiently described using the theory of random matrices [9, 32–40]. Alternative theoretical treatments of time delay in chaotic scattering systems successfully adopted a semiclassical approach, see [7] and references therein.

Despite the fact that standard theory of wave-chaotic scattering deals with perfectly flux-preserving systems,

^{*} LChen95@umd.edu

 $^{^{\}dagger}$ anlage@umd.edu

[‡] yan.fyodorov@kcl.ac.uk

in any actual realisation such systems are inevitably imperfect, hence absorbing, and theory needs to take this aspect into account [41]. Interestingly, studying scattering characteristics in a system with weak uniform (i.e. spatially homogeneous) losses may even provide a possibility to extract time delays characterizing idealized system without losses. This idea has been experimentally realized already in [17] which treated the effect of sub-unitary scattering by means of the unitary deficit of the S-matrix. In this case consider the Q-matrix defined through the relation $S^{\dagger}S = 1 - (\gamma \Delta/2\pi)Q_{UD}$, where γ is the dimensionless 'absorption rate' and Δ is the mean spacing between modes of the closed system. In the limit of vanishing absorption rate $\gamma \to 0$ such Q_{UD} can be shown to coincide with the Wigner-Smith time delay matrix for a lossless system, but formally one can extend this as a definition of Q for any $\gamma > 0$. Note that this version of time delay is always real and positive. Various statistical aspects of time delays in such and related settings were addressed theoretically in [42-45].

Experimental data is often taken on sub-unitary scattering systems and a straightforward use of the Wigner time delay definition yields a complex quantity. In addition, both the real and imaginary parts acquire both negative and positive values, and they show a systematic evolution with energy/frequency and other parameters of the scattering system. This clearly calls for a detailed theoretical understanding of this complex generalization of the Wigner time delay. It is necessary to stress that many possible definitions of time delays which are equivalent or directly related to each other in the case of a lossless flux-conserving systems can significantly differ in the presence of flux losses, either uniform or spatially localized. In the present paper we focus on a definition that can be directly linked to the fundamental characteristics of the scattering matrix - its poles and zeros in the complex energy plane, making it useful for fully characterizing an arbitrary scattering system. Note that S-matrix poles have been objects of long-standing theoretical [46–54] and experimental [21–23, 25] interest in chaotic wave scattering, whereas S-matrix zeroes started to attract research attention only recently [26, 55–63].

Complex Wigner Time Delay. In our exposition we use the framework of the so-called "Heidelberg Approach" to wave-chaotic scattering reviewed from different perspectives in [64, 65] and [66]. Let H be the $N \times N$ Hamil-

tonian which is used to model the closed system with ray-chaotic dynamics, W denoting the $N \times M$ matrix of coupling elements between the N modes of H and the M scattering channels, and by A the $N \times L$ matrix of coupling elements between the modes of H and the L localized absorbers, modelled as L absorbing channels. [67] The total unitary S-matrix, of size $(M + L) \times (M + L)$ describing both the scattering and absorption on equal footing, has the following block form, see e.g. [56]:

$$\mathcal{S}(E) = \begin{pmatrix} 1_M - 2\pi i W^\dagger D^{-1}(E) W & -2\pi i W^\dagger D^{-1}(E) A \\ -2\pi i A^\dagger D^{-1}(E) W & 1_L - 2\pi i A^\dagger D^{-1}(E) A \end{pmatrix}, \tag{1}$$

where we defined $D(E) = E - H + i(\Gamma_W + \Gamma_A)$ with $\Gamma_W = \pi W W^{\dagger}$ and $\Gamma_A = \pi A A^{\dagger}$.

The upper left diagonal $M \times M$ block of $\mathcal{S}(E)$ is the experimentally-accessible sub-unitary scattering matrix and is denoted as S(E). The presence of uniform-inspace absorption with strength γ can be taken into account by evaluating the S-matrix entries at complex energy: $S(E+i\gamma) := S_{\gamma}(E)$. The determinant of such a subunitary scattering matrix $S_{\gamma}(E)$ is then given by:

$$\det S_{\gamma}(E) := \det S(E + i\gamma) \tag{2}$$

$$= \frac{\det[E - H + i(\gamma + \Gamma_A - \Gamma_W)]}{\det[E - H + i(\gamma + \Gamma_A + \Gamma_W)]}$$
 (3)

$$=\prod_{n=1}^{N} \frac{E+i\gamma-z_n}{E+i\gamma-\mathcal{E}_n},\tag{4}$$

In the above expression we have used that the S-matrix zeros z_n are complex eigenvalues of the non-self-adjoint/non-Hermitian matrix $H+i(\Gamma_W-\Gamma_A)$, whereas the poles $\mathcal{E}_n=E_n-i\Gamma_n$ with $\Gamma_n>0$ are complex eigenvalues of yet another non-Hermitian matrix $H-i(\Gamma_W+\Gamma_A)$, frequently called in the literature "the effective non-Hermitian Hamiltonian" [9, 46, 54, 65, 66, 68]. Note that when localized absorption is absent, i.e. $\Gamma_A=0$, the zeros z_n and poles \mathcal{E}_n are complex conjugates of each other, as a consequence of S-matrix unitarity for real E and no uniform absorption $\gamma=0$. Extending to locally absorbing systems the standard definition of the Wigner delay time as the energy derivative of the total phase shift we now deal with a complex quantity:

$$\tau(E; A, \gamma) := \frac{-i}{M} \frac{\partial}{\partial E} \log \det S_{\gamma}(E)$$
 (5)

$$= \operatorname{Re} \tau(E; A, \gamma) + i \operatorname{Im} \tau(E; A, \gamma), \tag{6}$$

$$\operatorname{Re} \tau(E; A, \gamma) = \frac{1}{M} \sum_{n=1}^{N} \left[\frac{\operatorname{Im} z_n - \gamma}{(E - \operatorname{Re} z_n)^2 + (\operatorname{Im} z_n - \gamma)^2} + \frac{\Gamma_n + \gamma}{(E - E_n)^2 + (\Gamma_n + \gamma)^2} \right], \tag{7}$$

$$\operatorname{Im} \tau(E; A, \gamma) = -\frac{1}{M} \sum_{n=1}^{N} \left[\frac{E - \operatorname{Re} z_n}{(E - \operatorname{Re} z_n)^2 + (\operatorname{Im} z_n - \gamma)^2} - \frac{E - E_n}{(E - E_n)^2 + (\Gamma_n + \gamma)^2} \right]$$
(8)

Equation (7) for the real part is formed by two Lorentzians for each mode of the closed system, potentially with different signs. This is a striking difference from the case of the flux-preserving system in which the conventional Wigner time delay is expressed as a single Lorentzian for each resonance mode [69]. Namely, the first Lorentzian is associated with the nth zero while the second is associated with the corresponding pole of the scattering matrix. The widths of the two Lorentzians are controlled by system scattering properties, and when $\text{Im}z_n \to \gamma \pm 0$ the first Lorentzian in Eq. 7 acquires the divergent, delta-functional peak shape, of either positive or negative sign, centered at $E = \text{Re}z_n$. Note that the first term in Eq. 8 changes its sign at the same energy value. These properties are indicative of the "perfect resonance" condition, with divergence in the real part of the Wigner time delay signalling the wave/particle being perpetually trapped in the scattering environment. In different words, the energy of the incident wave/particle is perfectly absorbed by the system due to the finite losses.

The pair of equations (7, 8) forms the main basis for our consideration. In particular, we demonstrate in the Supp. Mat. Section I [70] that in the regime of well-resolved resonances Eqs. (7) and (8) can be used for extracting the positions of both poles and zeros in the complex plane from experimental measurements, provided the rate of uniform absorption γ is independently known. We would like to stress that in general the two Lorentzians in (7) are centered at different energies because generically the pole position E_n does not coincide with the real part of the complex zero $\text{Re}z_n$.

From a different angle it is worth noting that there is a close relation between the objects of our study and the phenomenon of the so called Coherent Perfect Absorption (CPA) which attracted considerable attention in recent years, both theoretically and experimentally [60, 62, 71–73]. Namely, the above-discussed match between the uniform absorption strength and the imaginary part of scattering matrix zero $\gamma = \text{Im} z_n$ simultaneously ensures the determinant of the scattering matrix to vanish, see Eq. (4). This is only possible when $|\psi_{\text{out}}\rangle = 0$ despite the fact that $|\psi_{\text{in}}\rangle \neq 0$, which is a manifestation of CPA, see e.g. [55, 56].

Experiment. We focus on experiments involving microwave graphs [13, 62, 74, 75] for a number of reasons. First, they provide for complex scattering scenarios with well-isolated modes amenable to detailed analysis. We thus avoid the complications of interacting poles and related interference effects [76]. Graphs also allow for convenient parametric control such as variable lumped lossy elements, variable global loss, and breaking of time-reversal invariance. We utilize an irregular tetrahedral microwave graph formed by coaxial cables and Tee-junctions, having M=2 single-mode ports, and broken time-reversal invariance. A voltage-controlled variable attenuator is attached to one internal node of the graph (see Fig. 1(a)), providing for a variable lumped loss (L=1, the control variable Γ_A). The nodes involv-

ing connections of the graph to the network analyzer, and the graph to the lumped loss, are made up of a pair of Tee-junctions. The coaxial cables and tee-junctions have a roughly uniform and constant attenuation produced by dielectric loss and conductor loss, which is parameterized by the uniform loss parameter γ . The 2-port graph has a total electrical length of $L_e=3.89$ m, a mean mode spacing of $\Delta=c/2L_e=38.5$ MHz, and a Heisenberg time $\tau_{\rm H}=2\pi/\Delta=163$ ns. The graph has equal coupling on both ports, characterized by a nominal value of $T_a=0.9450$ at a frequency of 2.6556 GHz. [77]

Comparison of Theory and Experiments. Figure 1 shows the evolution of complex time delay for a single isolated mode of the M=2 port tetrahedral microwave graph as Γ_A is varied. The complex time delay is evaluated as in Eq. 5 based on the experimental S(f) data, where f is the microwave frequency, a surrogate for energy E. Note that the (calibrated) measured S-parameter data is directly used for calculation of the complex time delay without any data pre-processing. The resulting real and imaginary parts of the time delay vary systematically with frequency, adopting both positive and negative values, depending on frequency and lumped loss in the graph. The full evolution animated over varying lumped loss is available in the Supplemental Material [70]. These variations are well-described by the theory given above.

Figure 1(d) and (e) clearly demonstrates that two Lorentzians are required to correctly describe the frequency dependence of the real part of the time delay. The two Lorentzians have different widths in general, given by the values of $\text{Im}z_n - \gamma$ and $\Gamma_n + \gamma$, and in this case the Lorentzians also have opposite sign. The frequency dependence of the imaginary part of the time delay also requires two terms, with the same parameters as for the real part, to be correctly described. The data in Fig. 1(b) also reveals that $Re[\tau]$ goes to very large positive values and suddenly changes sign to large negative values at a critical amount of local loss. For another attenuation setting of the same mode it was found that the maximum delay time was 337 times the Heisenberg time, showing that the signal resides in the scattering system for a substantial time.

The measured complex time delay as a function of frequency can be fit to Eqs. (7) and (8) to extract the corresponding pole and zero location for the S-matrix. The method to perform this fit is described in the Supp. Mat. Section I [70] The fitting parameters are $\operatorname{Re} z_n$ and $\operatorname{Im} z_n - \gamma$ for the zero, and E_n and $\Gamma_n + \gamma$ for the pole. Note that the $\operatorname{Re}[\tau(f)]$ and $\operatorname{Im}[\tau(f)]$ data are fit simultaneously, and constant offsets C_R and C_I are added to each fit.

Figure 2 summarizes the parameters required to fit the experimental complex time delay vs. frequency (shown in Fig. 1) as the localized loss due to the variable attenuator in the graph is increased. The significant feature here is the zero-crossing of $\text{Im} z_n - \gamma$ at frequency $f = f_{\text{CPA}}$, which corresponds to the point at which $\text{Re}[\tau(f)]$ changes sign. As shown in Fig. 2(a) this coincides with the point

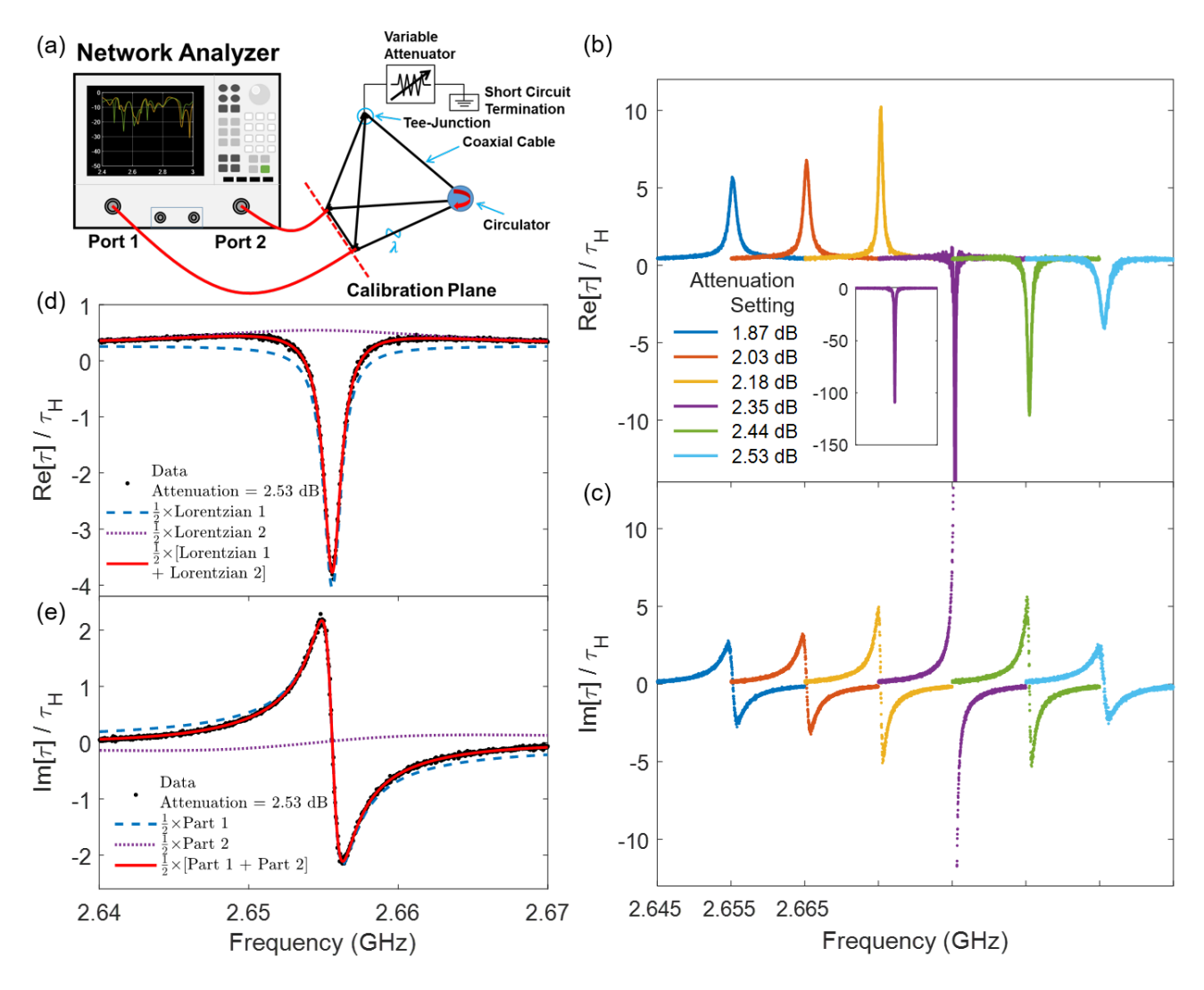


FIG. 1. (a) shows a schematic of the graph experimental setup. The lumped loss Γ_A is varied by changing the applied voltage to the variable attenuator. (b) and (c) show experimental data of both real and imaginary parts of Wigner time delay $\text{Re}[\tau]$ and $\text{Im}[\tau]$ (normalized by the Heisenberg time τ_{H}) as a function of frequency under different attenuation settings for a single isolated mode. For each attenuation setting, the data is plotted from 2.645 GHz to 2.665 GHz. For clarity, plots with higher attenuation setting are shifted 0.01 GHz from the previous one. Inset shows the entire range of $\text{Re}[\tau]$ for attenuation setting of 2.35 dB. (d) and (e) demonstrate the two-Lorentzian nature of the real and imaginary parts of the Wigner time delay as a function of frequency. The fitting parameters in these two plots are: $\text{Re}z_n = 2.6556$ GHz, $E_n = 2.6544$ GHz, $\text{Im}z_n - \gamma = -7.1065 \times 10^{-4}$ GHz, and $\Gamma_n + \gamma = 0.0110$ GHz. The constants used in the $\text{Re}[\tau]$ and $\text{Im}[\tau]$ fits are $C_R = 0.26$ and $C_I = -0.0018$ in units of τ_H . Detailed discussion about the fitting constants and degree of isolation of the modes can be found in the Supp. Mat. section IV [70].

at which $|\det(S(f))|$ achieves its minimum value at the CPA frequency f_{CPA} . This demonstrates that one or more eigenvalues of the S-matrix go through a complex zero value precisely as the condition $\text{Im}z_n - \gamma = 0$ and $f - \text{Re}z_n = 0$ is satisfied. Associated with this condition $|\text{Re}[\tau(f_{\text{CPA}})]|$ diverges, with corresponding large positive and negative values of $\text{Im}[\tau(f)]$ occurring just below and just above $f = f_{\text{CPA}}$. Similar behavior of $\text{Re}[\tau(f)]$ was recently observed in a complex scattering system containing re-configurable metasurfaces, as the pixels were toggled [73].

Next we wish to estimate the value of uniform attenua-

tion γ for the microwave graph. Using the unitary deficit of the S-matrix in a setup in which the attenuator is removed [17], we evaluate the uniform loss strength γ to be 3.73×10^{-3} GHz (see Supp. Mat. section III [70]).

Figure 2(b) summarizes the locations of the S-matrix pole \mathcal{E}_n and zero z_n of the single isolated mode of the microwave graph in the complex frequency plane as the localized loss is varied. When the S-matrix zero crosses the $\text{Im} z_n = \gamma$ value, one has the traditional signature of CPA. Note from Fig. 2 that the real parts of the zero and pole do not coincide and in fact move away from each other as localized loss is increased.

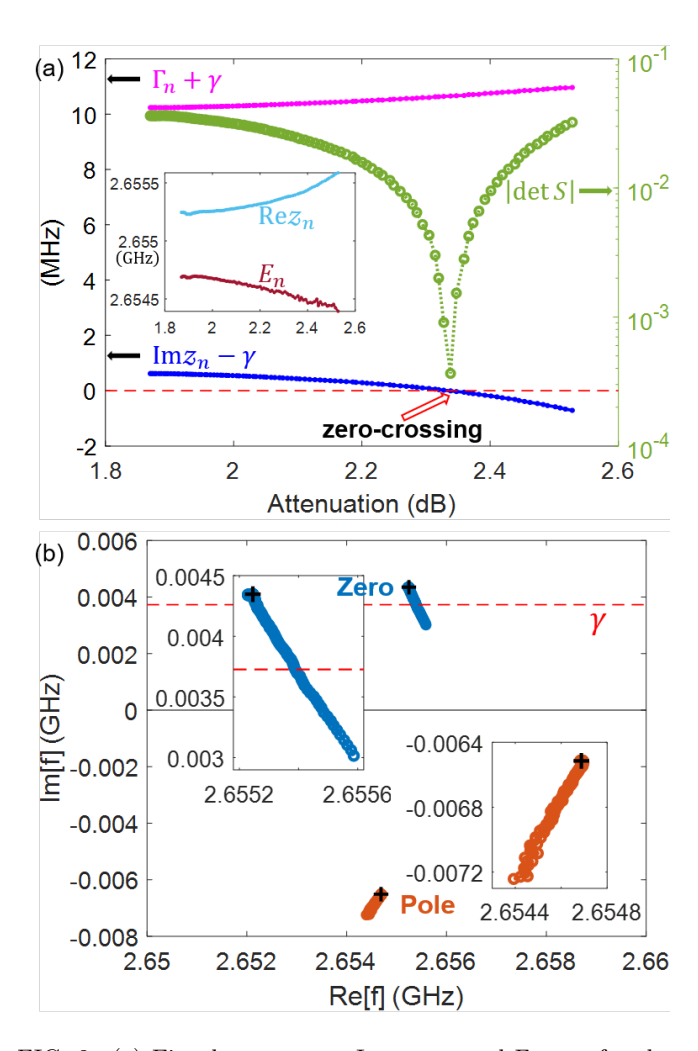


FIG. 2. (a) Fitted parameters $\mathrm{Im}z_n - \gamma$ and $\Gamma_n + \gamma$ for the complex Wigner time delay from graph experimental data. Also shown is the evolution of $|\det(S)|$ at the specific frequency of interest, f_{CPA} , which reaches its minimum at the zero-crossing point. Inset shows the evolution of $\mathrm{Re}z_n$ and $E_n = \mathrm{Re}\mathcal{E}_n$ with attenuation. (b) Evolution of complex zero and pole of a single mode of the graph in the complex frequency plane as a function of Γ_A . The black crosses are the initial state of the zero and pole at the minimum attenuation setting. Insets show the details of the complex zero and pole migrations.

Discussion. It should be noted that the occurrence of a negative real part of the time delay is an inevitable consequence of sub-unitary scattering, and is also expected for particles interacting with attractive potentials [78].

The imaginary part of time delay was in the past discussed in relation to changes in scattering unitary deficit with frequency [30]. Another approach to defining complex time delay has been recently suggested to be based on essentially calculating the time delay of the signal which comes out of the system without being absorbed

[73]. It should be noted that this ad hoc definition of time delay is not simply related to the poles and zeros of the S-matrix. Moreover, a closer inspection shows that such a definition of complex time delay tacitly assumes that the real parts of the pole and zero are identical. According to our theory such an assumption is incompatible with a proper treatment of localized loss.

We emphasize that the correct knowledge of the locations of the poles and zeros is essential for reconstructing the scattering matrix over the entire complex energy plane through Weierstrass factorization [79]. Through graph simulations presented in Sup. Mat. Section VII [70] we demonstrate that the complex time delay theory presented here also works for time-reversal invariant systems, and for systems with variable uniform absorption strength γ . Our results therefore establish a systematic procedure to find the S-matrix zeros and poles of isolated modes of a complex scattering system with an arbitrary number of coupling channels, symmetry class, and arbitrary degrees of both global and localized loss.

Recent work has demonstrated CPA in disordered and complex scattering systems [60, 62]. It has been discovered that one can systematically perturb such systems to induce CPA at an arbitrary frequency [73, 80], and this enables a remarkably sensitive detector paradigm [73]. These ideas can also be applied to optical scattering systems where measurement of the transmission matrix is possible [81]. Here we have uncovered a general formalism in which to understand how CPA can be created in an arbitrary scattering system. In particular this work shows that both the global loss (γ) , localized loss centers, or changes to the spectrum can be independently tuned to achieve the CPA condition.

Future work includes treating the case of overlapping modes, and the development of theoretical predictions for the statistical properties of both the real and imaginary parts of the complex time delay in chaotic and multiple scattering sub-unitary systems.

Conclusions. We have introduced a complex generalization of Wigner time delay which holds for arbitrary uniform/global and localized loss, and directly relates to poles and zeros of the scattering matrix in the complex energy/frequency plane. Based on that we developed theoretical expressions for complex time delay as a function of energy, and found very good agreement with experimental data on a sub-unitary complex scattering system. Time delay and $\det(S)$ share a common feature that CPA and the divergence of $\operatorname{Re}[\tau]$ and $\operatorname{Im}[\tau]$ coincide. This work opens a new window on time delay in lossy systems, enabling extraction of complex zeros and poles of the S-matrix from data.

We acknowledge Jen-Hao Yeh for early experimental work on complex time delay. This work was supported by AFOSR COE Grant No. FA9550-15-1-0171, NSF DMR2004386, and ONR Grant No. N000141912481.

- E. P. Wigner, Lower Limit for the Energy Derivative of the Scattering Phase Shift, Physical Review 98, 145 (1955).
- [2] F. T. Smith, Lifetime Matrix in Collision Theory, Physical Review 118, 349 (1960).
- [3] C. Texier, Wigner time delay and related concepts: Application to transport in coherent conductors, Physica E: Low-dimensional Systems and Nanostructures 82, 16 (2016).
- [4] S. Rotter, P. Ambichl, and F. Libisch, Generating Particlelike Scattering States in Wave Transport, Physical Review Letters 106, 120602 (2011).
- [5] J. Carpenter, B. J. Eggleton, and J. Schröder, Observation of Eisenbud--Wigner--Smith states as principal modes in multimode fibre, Nature Photonics 9, 751 (2015).
- [6] M. Horodynski, M. Kühmayer, A. Brandstötter, K. Pichler, Y. V. Fyodorov, U. Kuhl, and S. Rotter, Optimal wave fields for micromanipulation in complex scattering environments, Nature Photonics 14, 149 (2020).
- [7] J. Kuipers, D. V. Savin, and M. Sieber, Efficient semiclassical approach for time delays, New Journal of Physics 16, 123018 (2014).
- [8] M. Davy, Z. Shi, J. Wang, X. Cheng, and A. Z. Genack, Transmission Eigenchannels and the Densities of States of Random Media, Physical Review Letters 114, 033901 (2015).
- [9] Y. V. Fyodorov and H.-J. Sommers, Statistics of resonance poles, phase shifts and time delays in quantum chaotic scattering: Random matrix approach for systems with broken time-reversal invariance, Journal of Mathematical Physics 38, 1918 (1997).
- [10] F. Barra and P. Gaspard, Classical dynamics on graphs, Physical Review E 63, 066215 (2001).
- [11] H.-J. Stöckmann, Quantum Chaos: An Introduction (Cambridge University Press, 1999).
- [12] A. Richter, Wave dynamical chaos: An experimental approach in billiards, Physica Scripta T90, 212 (2001).
- [13] O. Hul, M. Lawniczak, S. Bauch, A. Sawicki, M. Kuś, and L. Sirko, Are Scattering Properties of Graphs Uniquely Connected to Their Shapes?, Physical Review Letters 109, 040402 (2012).
- [14] U. Kuhl, O. Legrand, and F. Mortessagne, Microwave experiments using open chaotic cavities in the realm of the effective Hamiltonian formalism, Fortschritte der Physik 61, 404 (2013).
- [15] G. Gradoni, J.-H. Yeh, B. Xiao, T. M. Antonsen, S. M. Anlage, and E. Ott, Predicting the statistics of wave transport through chaotic cavities by the random coupling model: A review and recent progress, Wave Motion 51, 606 (2014).
- [16] B. Dietz and A. Richter, Quantum and wave dynamical chaos in superconducting microwave billiards, Chaos: An Interdisciplinary Journal of Nonlinear Science 25, 097601 (2015).
- [17] E. Doron, U. Smilansky, and A. Frenkel, Experimental demonstration of chaotic scattering of microwaves, Physical Review Letters 65, 3072 (1990).
- [18] A. Z. Genack, P. Sebbah, M. Stoytchev, and B. A. Van Tiggelen, Statistics of wave dynamics in random media, Physical Review Letters 82, 715 (1999).

- [19] A. A. Chabanov, Z. Q. Zhang, and A. Z. Genack, Break-down of Diffusion in Dynamics of Extended Waves in Mesoscopic Media, Physical Review Letters 90, 203903 (2003).
- [20] H. Schanze, H.-J. Stöckmann, M. Martínez-Mares, and C. H. Lewenkopf, Universal transport properties of open microwave cavities with and without time-reversal symmetry, Physical Review E 71, 016223 (2005).
- [21] U. Kuhl, R. Höhmann, J. Main, and H.-J. Stöckmann, Resonance Widths in Open Microwave Cavities Studied by Harmonic Inversion, Physical Review Letters 100, 254101 (2008).
- [22] A. Di Falco, T. F. Krauss, and A. Fratalocchi, Lifetime statistics of quantum chaos studied by a multiscale analysis, Applied Physics Letters 100, 184101 (2012).
- [23] S. Barkhofen, T. Weich, A. Potzuweit, H.-J. Stöckmann, U. Kuhl, and M. Zworski, Experimental Observation of the Spectral Gap in Microwave n-Disk Systems, Physical Review Letters 110, 164102 (2013).
- [24] J.-B. Gros, U. Kuhl, O. Legrand, F. Mortessagne, E. Richalot, and D. V. Savin, Experimental Width Shift Distribution: A Test of Nonorthogonality for Local and Global Perturbations, Physical Review Letters 113, 224101 (2014).
- [25] C. Liu, A. Di Falco, and A. Fratalocchi, Dicke Phase Transition with Multiple Superradiant States in Quantum Chaotic Resonators, Physical Review X 4, 021048 (2014).
- [26] M. Davy and A. Z. Genack, Selectively exciting quasinormal modes in open disordered systems, Nature Communications 9, 4714 (2018).
- [27] S. Fan and J. M. Kahn, Principal modes in multimode waveguides, Optics Letters 30, 135 (2005).
- [28] W. Xiong, P. Ambichl, Y. Bromberg, B. Redding, S. Rotter, and H. Cao, Spatiotemporal Control of Light Transmission through a Multimode Fiber with Strong Mode Coupling, Physical Review Letters 117, 053901 (2016).
- [29] B. Gérardin, J. Laurent, P. Ambichl, C. Prada, S. Rotter, and A. Aubry, Particlelike wave packets in complex scattering systems, Physical Review B 94, 014209 (2016).
- [30] J. Böhm, A. Brandstötter, P. Ambichl, S. Rotter, and U. Kuhl, In situ realization of particlelike scattering states in a microwave cavity, Physical Review A 97, 021801(R) (2018).
- [31] P. Ambichl, A. Brandstötter, J. Böhm, M. Kühmayer, U. Kuhl, and S. Rotter, Focusing inside disordered media with the generalized Wigner–Smith operator, Physical Review Letters 119, 033903 (2017).
- [32] N. Lehmann, D. Savin, V. Sokolov, and H.-J. Sommers, Time delay correlations in chaotic scattering: random matrix approach, Physica D: Nonlinear Phenomena 86, 572 (1995).
- [33] V. A. Gopar, P. A. Mello, and M. Büttiker, Mesoscopic Capacitors: A Statistical Analysis, Physical Review Letters 77, 3005 (1996).
- [34] Y. V. Fyodorov, D. V. Savin, and H.-J. Sommers, Parametric correlations of phase shifts and statistics of time delays in quantum chaotic scattering: Crossover between unitary and orthogonal symmetries, Physical Review E 55, R4857(R) (1997).
- [35] P. W. Brouwer, K. Frahm, and C. W. J. Beenakker, Dis-

- tribution of the quantum mechanical time-delay matrix for a chaotic cavity, Waves Random Media 9, 91 (1999).
- [36] D. V. Savin, Y. V. Fyodorov, and H.-J. Sommers, Reducing nonideal to ideal coupling in random matrix description of chaotic scattering: Application to the time-delay problem, Physical Review E 63, 035202(R) (2001).
- [37] F. Mezzadri and N. J. Simm, Tau-Function Theory of Chaotic Quantum Transport with $\beta = 1, 2, 4$, Communications in Mathematical Physics **324**, 465 (2013).
- [38] C. Texier and S. N. Majumdar, Wigner time-delay distribution in chaotic cavities and freezing transition, Physical Review Letters 110, 250602 (2013).
- [39] M. Novaes, Statistics of time delay and scattering correlation functions in chaotic systems. I. Random matrix theory, Journal of Mathematical Physics 56, 062110 (2015).
- [40] F. D. Cunden, Statistical distribution of the Wigner– Smith time-delay matrix moments for chaotic cavities, Physical Review E 91, 060102(R) (2015).
- [41] Y. V. Fyodorov, D. V. Savin, and H.-J. Sommers, Scattering, reflection and impedance of waves in chaotic and disordered systems with absorption, Journal of Physics A: Mathematical and General 38, 10731 (2005).
- [42] C. Beenakker and P. Brouwer, Distribution of the reflection eigenvalues of a weakly absorbing chaotic cavity, Physica E: Low-dimensional Systems and Nanostructures 9, 463 (2001).
- [43] Y. V. Fyodorov, Induced vs. Spontaneous breakdown of S-matrix unitarity: Probability of no return in quantum chaotic and disordered systems, Journal of Experimental and Theoretical Physics Letters 78, 250 (2003).
- [44] D. V. Savin and H.-J. Sommers, Delay times and reflection in chaotic cavities with absorption, Physical Review E 68, 036211 (2003).
- [45] A. Grabsch, Distribution of the Wigner--Smith timedelay matrix for chaotic cavities with absorption and coupled Coulomb gases, Journal of Physics A: Mathematical and Theoretical 53, 025202 (2020).
- [46] V. Sokolov and V. Zelevinsky, Dynamics and statistics of unstable quantum states, Nuclear Physics A 504, 562 (1989).
- [47] F. Haake, F. Izrailev, N. Lehmann, D. Saher, and H.-J. Sommers, Statistics of complex levels of random matrices for decaying systems, Zeitschrift für Physik B Condensed Matter 88, 359 (1992).
- [48] Y. V. Fyodorov and H. J. Sommers, Statistics of S-matrix poles in few-channel chaotic scattering: Crossover from isolated to overlapping resonances, Journal of Experimental and Theoretical Physics Letters 63, 1026 (1996).
- [49] Y. V. Fyodorov and B. A. Khoruzhenko, Systematic Analytical Approach to Correlation Functions of Resonances in Quantum Chaotic Scattering, Physical Review Letters 83, 65 (1999).
- [50] H.-J. Sommers, Y. V. Fyodorov, and M. Titov, S-matrix poles for chaotic quantum systems as eigenvalues of complex symmetric random matrices: from isolated to overlapping resonances, Journal of Physics A: Mathematical and General 32, L77 (1999).
- [51] Y. V. Fyodorov and B. Mehlig, Statistics of resonances and nonorthogonal eigenfunctions in a model for single-channel chaotic scattering, Physical Review E 66, 045202(R) (2002).
- [52] C. Poli, D. V. Savin, O. Legrand, and F. Mortessagne, Statistics of resonance states in open chaotic systems: A perturbative approach, Physical Review E 80, 046203

- (2009).
- [53] G. L. Celardo, N. Auerbach, F. M. Izrailev, and V. G. Zelevinsky, Distribution of Resonance Widths and Dynamics of Continuum Coupling, Physical Review Letters 106, 042501 (2011).
- [54] Y. V. Fyodorov, Random matrix theory of resonances: An overview, in 2016 URSI International Symposium on Electromagnetic Theory (EMTS), Espoo, Finland (IEEE, 2016) pp. 666–669.
- [55] H. Li, S. Suwunnarat, R. Fleischmann, H. Schanz, and T. Kottos, Random matrix theory approach to chaotic coherent perfect absorbers, Physical Review Letters 118, 044101 (2017).
- [56] Y. V. Fyodorov, S. Suwunnarat, and T. Kottos, Distribution of zeros of the S-matrix of chaotic cavities with localized losses and coherent perfect absorption: non-perturbative results, Journal of Physics A: Mathematical and Theoretical 50, 30LT01 (2017).
- [57] D. G. Baranov, A. Krasnok, and A. Alù, Coherent virtual absorption based on complex zero excitation for ideal light capturing, Optica 4, 1457 (2017).
- [58] Y. V. Fyodorov, Reflection Time Difference as a Probe of S-Matrix Zeroes in Chaotic Resonance Scattering, Acta Physica Polonica A 136, 785 (2019).
- [59] A. Krasnok, D. Baranov, H. Li, M.-A. Miri, F. Monticone, and A. Alù, Anomalies in light scattering, Advances in Optics and Photonics 11, 892 (2019).
- [60] K. Pichler, M. Kühmayer, J. Böhm, A. Brandstötter, P. Ambichl, U. Kuhl, and S. Rotter, Random antilasing through coherent perfect absorption in a disordered medium, Nature 567, 351 (2019).
- [61] M. Osman and Y. V. Fyodorov, Chaotic scattering with localized losses: S-matrix zeros and reflection time difference for systems with broken time-reversal invariance, Physical Review E 102, 012202 (2020).
- [62] L. Chen, T. Kottos, and S. M. Anlage, Perfect absorption in complex scattering systems with or without hidden symmetries, Nature Communications 11, 5826 (2020).
- [63] M. F. Imani, D. R. Smith, and P. del Hougne, Perfect absorption in a disordered medium with programmable meta-atom inclusions, Advanced Functional Materials 30, 2005310 (2020).
- [64] G. E. Mitchell, A. Richter, and H. A. Weidenmüller, Random matrices and chaos in nuclear physics: Nuclear reactions, Reviews of Modern Physics 82, 2845 (2010).
- [65] Y. V. Fyodorov and D. V. Savin, Resonance scattering of waves in chaotic systems, in *The Oxford Handbook of Random Matrix Theory*, edited by G. Akemann, J. Baik, and P. D. Francesco (Oxford University Press, 2011) pp. 703–722.
- [66] H. Schomerus, Random matrix approaches to open quantum systems, in Stochastic Processes and Random Matrices: Lecture Notes of the Les Houches Summer School 2015, edited by G. Schehr, A. Altland, Y. V. Fyodorov, N. O'Connell, and L. F. Cugliandolo (Oxford University Press, 2017) pp. 409–473.
- [67] This way of modelling the localized absorbers as additional scattering channels is close in spirit to the so-called dephasing lead model of decoherence introduced in: M. Büttiker, Role of quantum coherence in series resistors, Phys. Rev. B 33, 3020 (1986) and further developed in P. W. Brouwer and C. W. J. Beenakker, Voltage-probe and imaginary-potential models for dephasing in a chaotic quantum dot, Phys. Rev. B 55, 4695 (1997).

- [68] I. Rotter, A non-Hermitian Hamilton operator and the physics of open quantum systems, Journal of Physics A: Mathematical and Theoretical 42, 153001 (2009).
- [69] V. Lyuboshitz, On collision duration in the presence of strong overlapping resonance levels, Physics Letters B 72, 41 (1977).
- [70] See Supplemental Material at [URL will be inserted by publisher] for the details of extracting poles and zeros from data, the sign convention used for the scattering matrix frequency evolution, evaluation of the system uniform loss strength γ , discussions about effects of neighboring resonances on fitting to the complex time delay, further details about CPA and complex time delay, connections to earlier work on negative real time delay and imaginary time delay, simulations of time-reversal invariant graphs and evaluation of complex time delay with varying uniform loss, and for animations of time delay evolution with variation of lumped loss (experiment Fig. 1 (b) and (c)) or uniform loss (simulation Fig. S4 (b) and (c)).
- [71] Y. D. Chong, L. Ge, H. Cao, and A. D. Stone, Coherent Perfect Absorbers: Time-Reversed Lasers, Physical Review Letters 105, 053901 (2010).
- [72] D. G. Baranov, A. Krasnok, T. Shegai, A. Alù, and Y. Chong, Coherent perfect absorbers: linear control of light with light, Nature Reviews Materials 2, 17064 (2017).
- [73] P. del Hougne, K. B. Yeo, P. Besnier, and M. Davy, On-demand coherent perfect absorption in complex scattering systems: time delay divergence and enhanced sensitivity to perturbations (2020), arXiv:2010.06438 [physics.class-ph].

- [74] O. Hul, S. Bauch, P. Pakoński, N. Savytskyy, K. Życzkowski, and L. Sirko, Experimental simulation of quantum graphs by microwave networks, Physical Review E 69, 056205 (2004).
- [75] M. Lawniczak, O. Hul, S. Bauch, P. Seba, and L. Sirko, Experimental and numerical investigation of the reflection coefficient and the distributions of Wigner's reaction matrix for irregular graphs with absorption, Physical Review E 77, 056210 (2008).
- [76] E. Persson, K. Pichugin, I. Rotter, and P. Šeba, Interfering resonances in a quantum billiard, Physical Review E 58, 8001 (1998).
- [77] The coupling strength T_a is determined by the value of the radiation S-matrix ($T_a = 1 |S_{\text{rad}}|^2$). The radiation S is measured when the graph is replaced by 50 Ω loads connected to the three output connectors of each node attached to the network analyzer test cables.
- [78] U. Smilansky, Delay-time distribution in the scattering of time-narrow wave packets. (I), Journal of Physics A: Mathematical and Theoretical 50, 215301 (2017).
- [79] V. Grigoriev, A. Tahri, S. Varault, B. Rolly, B. Stout, J. Wenger, and N. Bonod, Optimization of resonant effects in nanostructures via Weierstrass factorization, Physical Review A 88, 011803(R) (2013).
- [80] B. W. Frazier, T. M. Antonsen, S. M. Anlage, and E. Ott, Wavefront shaping with a tunable metasurface: Creating cold spots and coherent perfect absorption at arbitrary frequencies, Physical Review Research 2, 043422 (2020).
- [81] S. M. Popoff, G. Lerosey, R. Carminati, M. Fink, A. C. Boccara, and S. Gigan, Measuring the Transmission Matrix in Optics: An Approach to the Study and Control of Light Propagation in Disordered Media, Physical Review Letters 104, 100601 (2010).

SUPPLEMENTARY MATERIAL for Generalization of Wigner Time Delay to Sub-Unitary Scattering Systems

Lei Chen,^{1,2} Steven M. Anlage,^{1,2} and Yan V. Fyodorov^{3,4}

¹Quantum Materials Center, Department of Physics, University of Maryland, College Park, MD 20742, USA

²Department of Electrical and Computer Engineering,

University of Maryland, College Park, MD 20742, USA

³Department of Mathematics, King's College London, London WC26 2LS, United Kingdom
⁴L. D. Landau Institute for Theoretical Physics, Semenova 1a, 142432 Chernogolovka, Russia
(Dated: April 27, 2021)

We provide some additional details for some of the calculations described in the text of the Letter.

I. EXTRACTING POLES AND ZEROS FROM EXPERIMENTAL DATA

Consider a pair of single terms in the sum over n in Eqs. (7–8)

$$\operatorname{Re}\tau_n(f) = \left[\frac{\operatorname{Im}z_n - \gamma}{(f - \operatorname{Re}z_n)^2 + (\operatorname{Im}z_n - \gamma)^2} + \frac{\Gamma_n + \gamma}{(f - E_n)^2 + (\Gamma_n + \gamma)^2}\right],\tag{S1}$$

$$-\operatorname{Im} \tau_n(f) = \left[\frac{f - \operatorname{Re} z_n}{(f - \operatorname{Re} z_n)^2 + (\operatorname{Im} z_n - \gamma)^2} - \frac{f - E_n}{(f - E_n)^2 + (\Gamma_n + \gamma)^2} \right]$$
(S2)

where we 'relabeled' the energy parameter E as 'frequency' f.

Extracting the parameters $\operatorname{Re} z_n, \operatorname{Im} z_n, E_n, \Gamma_n$ and the uniform absorption strength γ from the experimentally measured curves $\operatorname{Im} \tau_n(f)$ and $\operatorname{Re} \tau_n(f)$ is possible by the following procedure.

1. Let us **define** the "resonance frequency" value $f = f^*$ by the condition

$$\operatorname{Im} \tau_n(f^*) = 0 \tag{S3}$$

2. Measure from the two above curves the following 3 parameters:

$$s = -\frac{d}{df}\operatorname{Im}\tau_n(f)|_{f=f^*}, \quad m = \operatorname{Re}\tau_n(f^*), \quad \delta = -\frac{1}{2}\frac{d}{df}\operatorname{In}\left[\operatorname{Re}\tau_n(f)\right]|_{f=f^*}$$
 (S4)

and use them to build combinations:

$$\alpha_{-} = \frac{1}{2} \left(-\frac{s}{m} + m \right), \quad \alpha_{+} = \frac{1}{2} \left(\frac{s}{m} + m \right) \tag{S5}$$

The following relations then can be derived for the positions of resonance poles and zeros.

For the real parts:

$$E_n = f^* - \frac{\delta}{\delta^2 + \alpha_-^2}, \quad \text{Re } z_n = f^* - \frac{\delta}{\delta^2 + \alpha_+^2}$$
 (S6)

For the imaginary parts:

$$\Gamma_n = -\gamma + \frac{\alpha_-}{\delta^2 + \alpha_-^2}, \quad \text{Im } z_n = \gamma + \frac{\alpha_+}{\delta^2 + \alpha_+^2}$$
 (S7)

Derivation of relations (S6)-(S7)

Define for brevity $x_n := f^* - \operatorname{Re} z_n$, $r_n := \operatorname{Im} z_n - \gamma$, $\epsilon_n := f^* - E_n$ and $p_n := \Gamma_n + \gamma$.

Then condition (S3) implies

$$\frac{x_n}{x_n^2 + r_n^2} = \frac{\epsilon_n}{\epsilon_n^2 + p_n^2} \tag{S8}$$

Also we have by the definition

$$m = \text{Re}\,\tau_n(f)|_{f=f^*} = \frac{r_n}{x_n^2 + r_n^2} + \frac{p_n}{\epsilon_n^2 + p_n^2}$$
 (S9)

On the other hand differentiating (S2) gives with this notation:

$$s = -\frac{d}{df} \operatorname{Im} \tau_n(f)|_{f=f^*} = \frac{r_n^2 - x_n^2}{(x_n^2 + r_n^2)^2} - \frac{p_n^2 - \epsilon_n^2}{(p_n^2 + \epsilon_n^2)^2}$$
(S10)

Now using the condition (S8) the above equation simplifies to

$$s = \frac{r_n^2}{(x_n^2 + r_n^2)^2} - \frac{p_n^2}{(p_n^2 + \epsilon_n^2)^2} = \left[\frac{r_n}{(x_n^2 + r_n^2)} - \frac{p_n}{(p_n^2 + \epsilon_n^2)} \right] \left[\frac{r_n}{(x_n^2 + r_n^2)} + \frac{p_n}{(p_n^2 + \epsilon_n^2)} \right]$$
(S11)

which after using (S9) gives

$$s/m = \left[\frac{r_n}{(x_n^2 + r_n^2)} - \frac{p_n}{(p_n^2 + \epsilon_n^2)} \right]$$
 (S12)

Now the pair (S9)–(S12) implies

$$\alpha_{+} := \frac{1}{2} \left(\frac{s}{m} + m \right) = \frac{r_n}{x_n^2 + r_n^2}, \quad \alpha_{-} := \frac{1}{2} \left(-\frac{s}{m} + m \right) = \frac{p_n}{p_n^2 + \epsilon_n^2}$$
 (S13)

Finally, let us consider

$$-\frac{1}{2}\frac{d}{df}\operatorname{Re}\tau_n(f)|_{f=f^*} = \frac{r_n x_n}{(x_n^2 + r_n^2)^2} + \frac{p_n \epsilon_n}{(p_n^2 + \epsilon_n^2)^2}$$
(S14)

which after first using (S8) and then (S9) can be further rewritten as

$$=\frac{\epsilon_n}{p_n^2+\epsilon_n^2}\left[\frac{r_n}{x_n^2+r_n^2}+\frac{p_n}{p_n^2+\epsilon_n^2}\right]=\frac{\epsilon_n}{p_n^2+\epsilon_n^2}\mathrm{Re}\,\tau_n(f)|_{f=f^*}$$

implying finally

$$\delta := -\frac{1}{2} \frac{d}{df} \ln \left[\text{Re} \, \tau_n(f) \right] |_{f = f^*} = \frac{\epsilon_n}{p_n^2 + \epsilon_n^2} = \frac{r_n}{x_n^2 + r_n^2} \tag{S15}$$

The pair of equations (S13) and (S15) can be easily solved and gives (S6)–(S7).

So the only parameter which remains to be found from independent measurement is the uniform absorption γ .

Note: Note that generically both $s = -\frac{d}{df} \operatorname{Im} \tau_n(f)|_{f=f^*} \neq 0$ and $m = \operatorname{Re} \tau_n(f)|_{f=f^*} \neq 0$ so $|\alpha_+| \neq |\alpha_-|$. We then see from Eq. (S6) that to have $E_n = \operatorname{Re} z_n$ is only possible if $\delta = 0$, which in turn is only possible if $\frac{d}{df} [\operatorname{Re} \tau_n(f)]|_{f=f^*} = 0$. The latter condition would mean that the maximum or minimum on the curve $\operatorname{Re} \tau_n(f)$ happens exactly at the same frequency f^* where the imaginary part vanishes. Generically this never happens due to the two-Lorentzian nature of $\operatorname{Re} \tau_n(f)$.

II. SIGN CONVENTION FOR THE PHASE EVOLUTION OF THE S-MATRIX ELEMENTS

It should be noted that there are two widely-used conventions for the evolution of the phase of the complex S-matrix elements with increasing frequency. Microwave network analyzers utilize a convention in which the phase of the scattering matrix elements decreases with increasing frequency. Here we adopt the convention used in the theoretical literature that the phase of S-matrix elements increases with increasing frequency.

III. EVALUATION OF SYSTEM UNIFORM LOSS STRENGTH γ

The value of γ is estimated in a situation in which the uniform attenuation of the coaxial cables dominates the overall loss of the system. These losses arise from metallic and dielectric loss in the cables and are quite homogeneously distributed in the system. Here we estimate the value of uniform attenuation γ for the microwave graph using the unitary deficit of the S-matrix [1]. We measured the graph with the variable attenuator removed (see Fig. 1(a) in the main text), and measured the 2×2 S-matrix under this no-attenuator condition. The unitary deficit of the S-matrix is expected to be $\ln |\det S| \approx -M\gamma \text{Re}[\tau]$ in the limit of low loss [1], where M is the number of channels (M=2) in this paper). Fig. S1 shows the det S and $\text{Re}[\tau]$ versus frequency experimental data for the resonance of interest when no attenuator is present. The linear fitting function in Fig. S1(b) determines the uniform loss strength to be $\gamma = 3.73 \times 10^{-3}$ GHz.

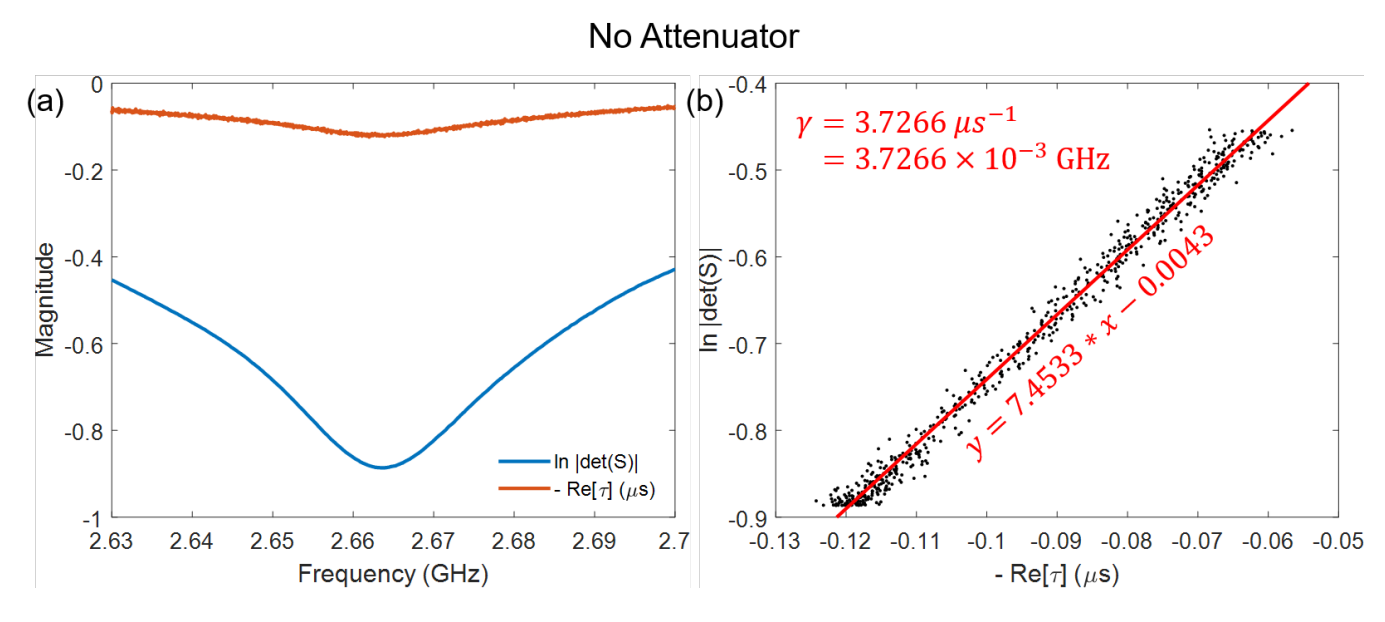


FIG. S1. (a) Measurement of $\ln |\det S|$ and $-\operatorname{Re}[\tau]$ as a function of frequency for the resonance of interest in a no-attenuator tetrahedral graph. (b) Plot of $\ln |\det S|$ vs. $-\operatorname{Re}[\tau]$ (with frequency as a parameter) and a linear fit between these two quantities to evaluate the uniform loss strength γ .

IV. EFFECTS OF NEIGHBORING RESONANCES

In this paper we use an isolated mode for data fitting and analysis. A good definition of 'isolated resonance' is that the separation is much larger than the width of the resonance. Fig. S2 shows the separation between the mode fit in the main text and its neighboring resonances, where the nearest-neighbor distance for the middle resonance is $\Delta f = 0.0393$ GHz (with the resonance on the right). Under this attenuation setting, the resonance widths of the two Lorentzians from the zero and pole for the middle resonance are $|\text{Im}z_n - \gamma| = 7.1065 \times 10^{-4}$ GHz and $\Gamma_n + \gamma = 0.0110$ GHz, which give rise to dimensionless separation estimates of $\frac{\Delta f}{|\text{Im}z_n - \gamma|} = 55.3$ and $\frac{\Delta f}{\Gamma_n + \gamma} = 3.6$, respectively.

In situations where the isolation between neighboring resonances is not large, the nearby resonances may have some contributions to the complex time delay at the resonance of interest. Here we evaluate this effect by using Eqs. (7) and (8) of the main text for three hypothetical modes. We utilize three similar pairs of zero and pole with adjustable mode spacing between them (see Fig. S3). The middle resonance has the same zero and pole from the experimental data, and the neighboring two resonances have the same information except for the variable frequency separation between them. Fig. S3 clearly demonstrates that the neighboring resonances can have strong background contributions to Re[τ], which may lead to a non-negligible constant C_R in the fitting process (see Fig. 1(d) and (e) in the main text and Fig. S4(d) and (e) in the Supp. Mat. section VII). The contribution to Im[τ], on the other hand, is quite small because Imτ changes sign through the resonance, hence for a low density of modes the 'tails' of the Im[τ] contributions cancel out to good approximation. Fig. S3(d) shows the background contribution τ_{Bkd} to Re[τ] and Im[τ] at the resonance of interest as a function of the mode separation. Clearly Re[τ] is more sensitive to the

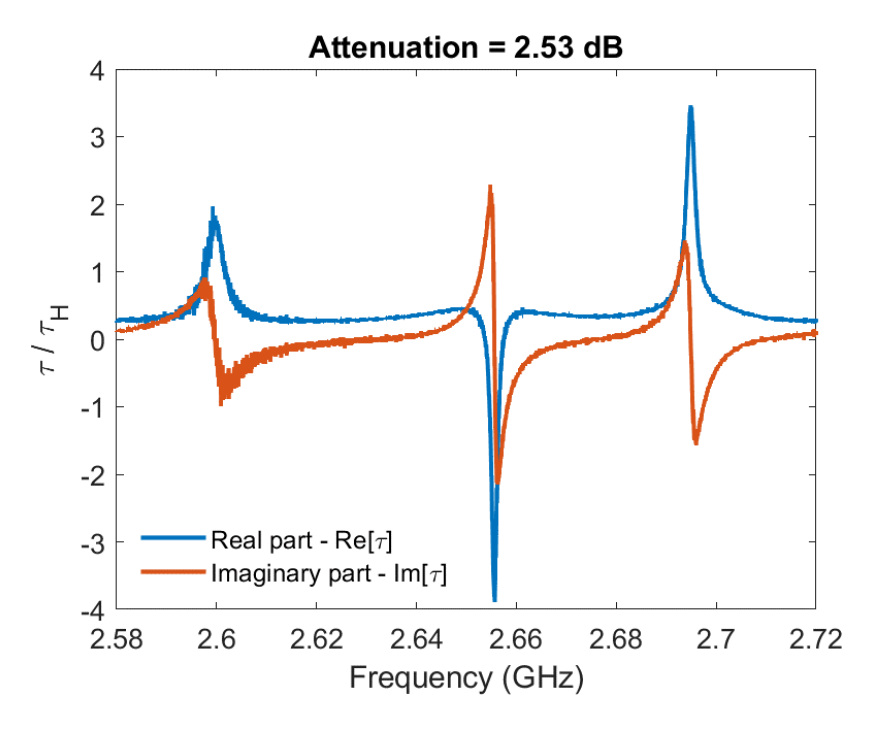


FIG. S2. Complex time delay experimental data for the neighboring resonances at an attenuation setting of 2.53 dB. The resonance mode in the middle is the one being analyzed in the main text.

presence of nearby modes and requires larger fit values for $C_{\rm R}$, as compared to $C_{\rm I}$, consistent with the results in Fig. 1 of the main text.

V. FURTHER DETAILS ABOUT CPA AND COMPLEX TIME DELAY

We note that at CPA both the peak in $|\text{Re }\tau|$ and the point at which Im τ changes its sign coincide in energy, but away from CPA these features may occur at different energies. Note that the real and imaginary parts share the same forms in the denominator of the Lorentzians. This leads to a synchronous evolution of their shapes with energy and scattering characteristics. This property is clearly demonstrated in both the data shown in the main text and in the simulations below in Section VII.

We also note that CPA can be achieved by tuning either localized loss Γ_A , or uniform loss γ , as demonstrated in Fig. 2 of the main text and Fig. S5 of Supp. Mat. Section VII, respectively.

VI. CONNECTIONS TO EARLIER WORK ON NEGATIVE REAL TIME DELAY AND IMAGINARY TIME DELAY

In the past, the concept of a complex transmission delay was developed in the context of principal modes in multimode waveguides [2], and a similar quantity was later used in the experimental realization of particle-like scattering states [3]. Complex dwell time was defined for a multiple scattering medium with lossy resonant absorbers [4].

An early study of Gaussian pulse propagation through an anomalously dispersive medium predicted negative delay [5], and later measurements confirmed the theory [6]. The observed negative delay of the pulse was attributed to the fact that the leading edge of the pulse is attenuated less than the later parts, and the Gaussian shape is approximately preserved, under appropriate circumstances. Negative real parts of reflection delay time have been measured experimentally in a one-dimensional Levy-flight system but were dismissed as an artefact due to prompt reflections [7].

Our findings show that in general the real part of the delay as a function of frequency is not symmetric about the resonance as a consequence of the differences in the real parts of z_n and \mathcal{E}_n , and that it has a distinctive two-Lorentzian character that had not been appreciated until now.

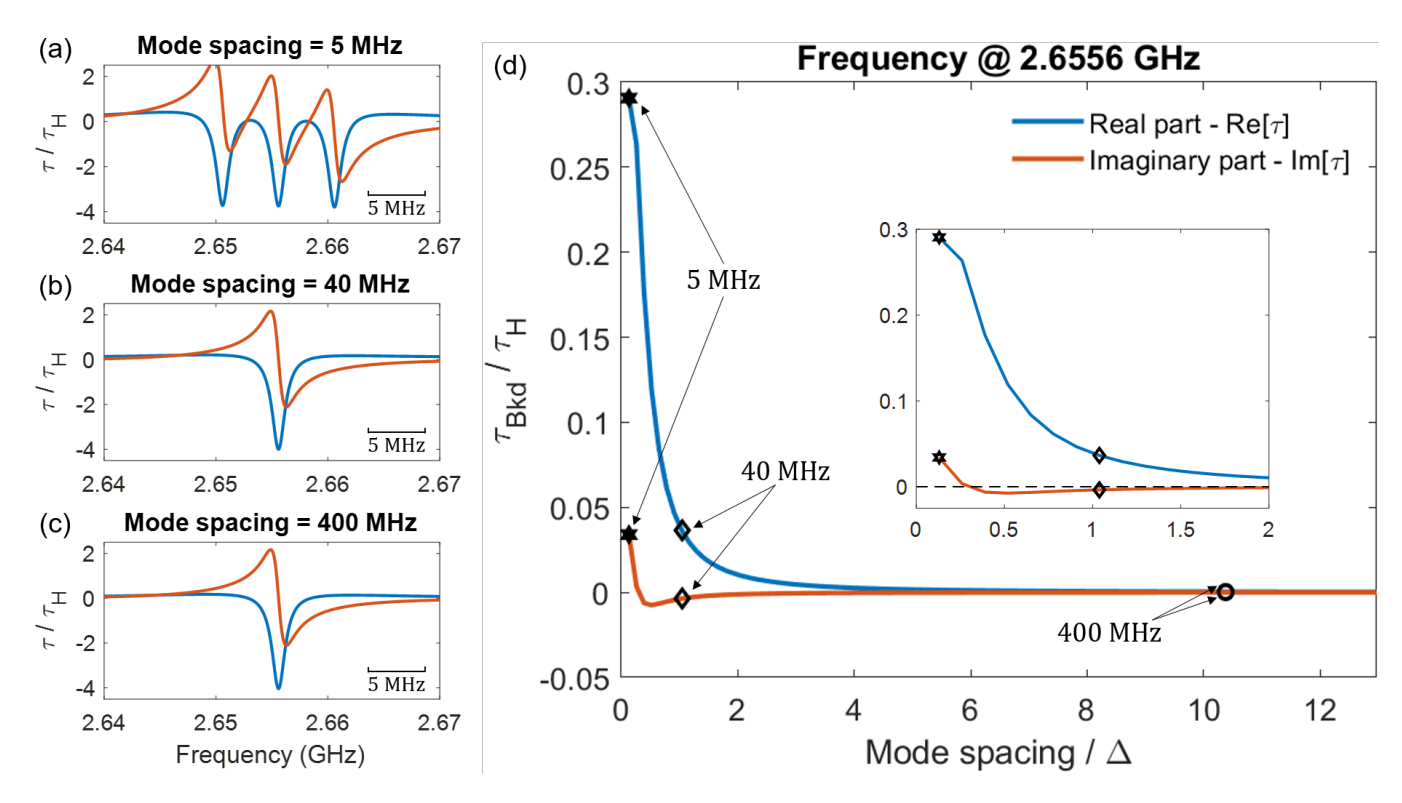


FIG. S3. Simulations based on Eqs. (7) and (8) of the main text of the effect of neighboring resonances on the background values $\tau_{\rm Bkd}$ of Re[τ] and Im[τ] at the location of the center resonance. (a)–(c) show the complex time delay for three constructed neighboring resonances with variable mode spacing. A scale bar of 5 MHz is added for reference. Here $\tau_{\rm H}=163$ ns is the Heisenberg time from the experiment discussed in the main text. The parameters used for the center resonance are: Re $z_n=2.6556$ GHz, $E_n=2.6544$ GHz, Im $z_n-\gamma=-7.1065\times 10^{-4}$ GHz, and $\Gamma_n+\gamma=0.0110$ GHz. (d) shows the background contributions $\tau_{\rm Bkd}$ of both the real and imaginary parts of complex time delay from the neighboring two resonances at the center frequency of 2.6556 GHz. Here $\Delta=38.5$ MHz is the mean mode spacing of the experimental graph in the main text, and is simply used as a characteristic frequency scale for normalization. The corresponding data points from (a) – (c) are labelled in the plot. The background contributions decrease dramatically as the mode spacing increases, and the background contribution to Im[τ] is much smaller compared with the contribution to Re[τ]. Inset in (d) shows a zoom-in view of the two contributions for small mode spacing.

VII. SIMULATIONS OF GRAPHS AND EVALUATION OF COMPLEX TIME DELAY

We have simulated the microwave graphs using CST Microwave Studio utilizing an idealized simulation model. In this model, an irregular tetrahedral graph similar to that used in the experiment is considered. The graph nodes are represented by Tee-junctions which are set to be ideal (point-like with an ideal scattering matrix), and the only source of loss in the setup comes from uniform dielectric loss of the coaxial cables which can be conveniently varied by changing the dielectric loss parameter $\tan \delta$. The 2-port graph simulation model has a total electrical length of 8.69 m, Heisenberg time $\tau_{\rm H}=364$ ns, equal coupling on both ports, characterized by a nominal value of $T_a=0.75$, and no lumped loss (i.e. $\Gamma_A=0$). Note that in contrast to the experiment discussed in the main text, here we consider a time-reversal invariant microwave graph. This is done, in part, to demonstrate that the complex time delay theory applies to all classes of complex scattering systems.

The new insight created by the simulation comes from the ability to systematically vary the uniform loss γ while keeping all other parameters fixed. In this way we can show how CPA can be accomplished by simply changing the uniform loss. Results are shown in Figs. S4 and S5, which are similar to the experimental results Figs. 1 and 2 in the main text. The CPA condition is achieved for a single isolated mode at $f_{\text{CPA}} = 6.15265$ GHz when the uniform loss tangent value is tuned through a value of $\tan \delta = 7.8 \times 10^{-6}$.

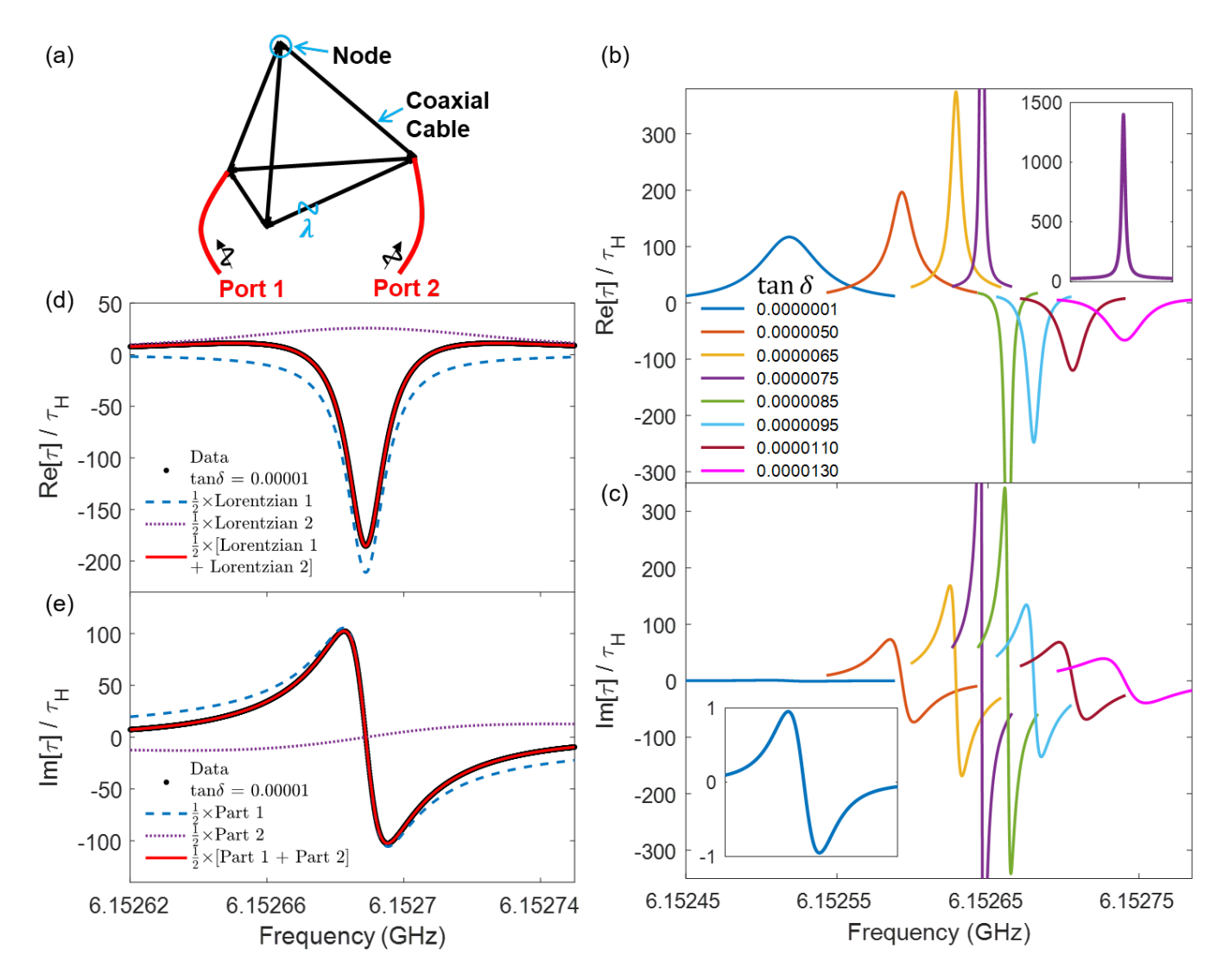


FIG. S4. Complex Wigner time delay from graph simulation with varying uniform loss γ . (a) shows a schematic of the graph simulation setup. The uniform loss γ is varied by changing the dielectric loss parameter $\tan\delta$ of the coaxial cables. (b) and (c) show simulation data of both real and imaginary parts of Wigner time delay $\text{Re}[\tau]$ and $\text{Im}[\tau]$ (normalized by the Heisenberg time τ_{H}), as a function of frequency under different uniform loss settings for a single isolated mode near 6.1526 GHz. Inset in (b) shows the entire range of $\text{Re}[\tau]$ for $\tan\delta = 7.5 \times 10^{-6}$, and inset in (c) shows the zoom-in view of $\text{Im}[\tau]$ for $\tan\delta = 10^{-7}$. (d) and (e) demonstrate the two-Lorentzian nature of the real and imaginary parts of the Wigner time delay (normalized by the Heisenberg time τ_{H}) as a function of frequency. The fitting parameters in these two plots are: $\text{Re}z_n = 6.1527$ GHz, $E_n = 6.1527$ GHz, and $E_n = 6.1527$ GHz. The constants used in the $E_n = 6.1527$ GHz are $E_n = 6.1527$ GHz in units of $E_n = 6.1527$ GHz.

VIII. ANIMATIONS OF TIME DELAY EVOLUTION WITH VARIATION OF SYSTEM PARAMETERS

Animation of experimental $\text{Re}[\tau(f)]$ and $\text{Im}[\tau(f)]$ as lumped loss is varied through the CPA condition. Animation of simulation $\text{Re}[\tau(f)]$ and $\text{Im}[\tau(f)]$ as uniform loss γ is varied through the CPA condition.

^[1] E. Doron, U. Smilansky, and A. Frenkel, Experimental demonstration of chaotic scattering of microwaves, Physical Review Letters 65, 3072 (1990).

^[2] S. Fan and J. M. Kahn, Principal modes in multimode waveguides, Optics Letters 30, 135 (2005).

^[3] J. Böhm, A. Brandstötter, P. Ambichl, S. Rotter, and U. Kuhl, In situ realization of particlelike scattering states in a

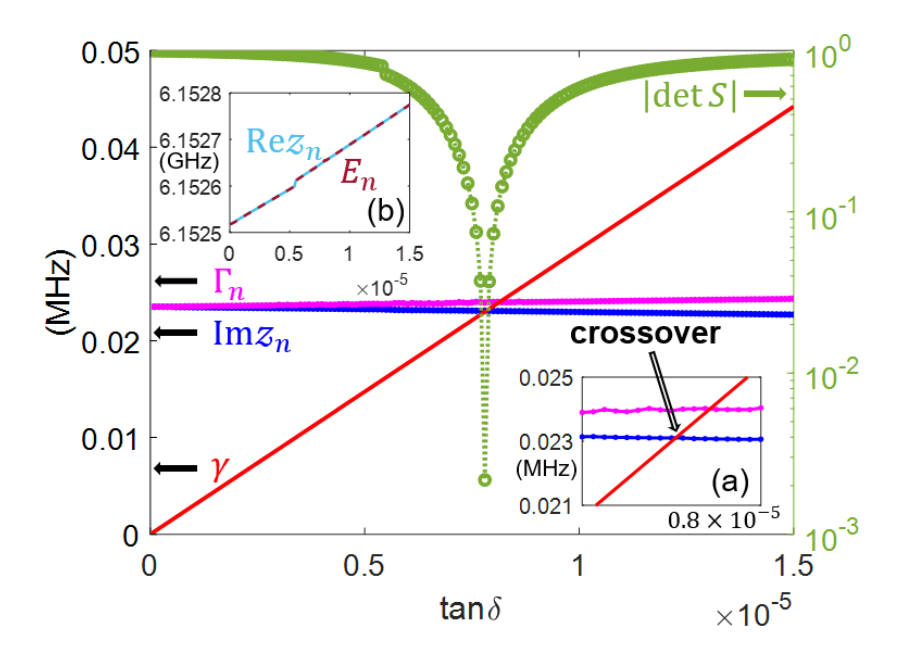


FIG. S5. Evolution of scattering matrix zero and pole for a single mode in the graph simulation with varying uniform loss γ . Plot shows the fitted parameters $\mathrm{Im} z_n$ and Γ_n for the complex Wigner time delay from graph simulation data. Also shown is the evolution of $|\det(S)|$ at the specific frequency of interest, f_{CPA} , which reaches its minimum at the crossover point where $\mathrm{Im} z_n - \gamma = 0$. Inset (a) shows the zoom-in details of the crossover when $\mathrm{Im} z_n$ matches with γ , and inset (b) shows the evolution of $\mathrm{Re} z_n$ and $E_n = \mathrm{Re} \mathcal{E}_n$ with varying $\mathrm{tan} \delta$. In this case, the real part of zero and pole are equal.

microwave cavity, Physical Review A 97, 021801(R) (2018).

- [4] M. Durand, S. M. Popoff, R. Carminati, and A. Goetschy, Optimizing light storage in scattering media with the dwell-time operator, Physical Review Letters 123, 243901 (2019).
- [5] C. G. B. Garrett and D. E. McCumber, Propagation of a gaussian light pulse through an anomalous dispersion medium, Physical Review A 1, 305 (1970).
- [6] S. Chu and S. Wong, Linear pulse propagation in an absorbing medium, Physical Review Letters 48, 738 (1982).
- [7] L. A. Razo-López, A. A. Fernández-Marín, J. A. Méndez-Bermúdez, J. Sánchez-Dehesa, and V. A. Gopar, Delay time of waves performing lévy walks in 1d random media, Scientific reports 10, 20816 (2020).